Coulomb distortion and medium corrections in nucleon-removal reactions

M. Karakoc,[1,4,*] A. Banu,[2] C. A. Bertulani,[1] and L. Trache[3]
[1]*Department of Physics & Astronomy, Texas A&M University—Commerce, Commerce, Texas 75428, USA*
[2]*Department of Physics & Astronomy, James Madison University, Harrisonburg, Virginia 22807, USA*
[3]*Cyclotron Institute, Texas A&M University, College Station, Texas 77843, USA*
[4]*Department of Physics, Akdeniz University, TR 07058 Antalya, Turkey*
(Received 17 January 2012; revised manuscript received 28 January 2013; published 19 February 2013)

Background: One-nucleon removal reactions at or above the Fermi energy are important tools to explore the single-particle structure of exotic nuclei. Experimental data must be compared with calculations to extract structure information, evaluate correlation effects in nuclei, or determine reaction rates for nuclear astrophysics. However, there is insufficient knowledge to calculate the cross sections for these reactions accurately.
Purpose: We evaluate the contributions of the final-state interaction (FSI) and of the medium modifications of the nucleon-nucleon interactions and obtain the shapes and magnitudes of the momentum distributions. Such effects have been often neglected in the literature.
Method: Calculations for reactions at energies of 35–1000 MeV/nucleon are reported and compared to published data. For consistency, the state-of-the-art eikonal method for stripping and diffraction dissociation is used.
Results: We find that the two effects are important and their relative contributions vary with the energy and with the atomic and mass number of the projectile involved.
Conclusions: These two often neglected effects modify considerably the one-nucleon-removal cross sections. As expected, the effects are largest at lower energies, around 50 MeV/nucleon, and on heavy targets.

DOI: 10.1103/PhysRevC.87.024607 PACS number(s): 25.60.Gc, 21.65.−f, 21.10.Jx

I. INTRODUCTION

Nucleon knockout reactions in nuclear collisions at and above the Fermi energy in nuclei have become an important tool to determine the occupancy of single-particle states and the correlation effects in the nuclear many-body system (see, e.g., Refs. [1–5]). In peripheral, sudden collisions of fast-moving projectiles with a target nucleus, a single nucleon is removed from the projectile, producing projectile-like residues in the exit channel, which are measured. Referred to the center-of-mass system of the projectile, the transferred momentum is $\mathbf{k}_c$. For the knockout reactions in the sudden approximation, this must equal the momentum of the struck nucleon before the collision. The standard reaction models assume that the ground state of the projectile of spin and parity J^π can be approximated by a superposition of configurations of the form $[I_c^{\pi_c} \otimes nlj]^{J^\pi}$, where $I_c^{\pi_c}$ denote the core states and the nlj are the quantum numbers for the single-particle wave functions in a spherical mean-field potential. The measured partial cross sections to individual final levels c of the core allow us to extract, by comparison with theoretical calculations, the spectroscopic factors for the individual core–single-particle configurations. In complete analogy to the use of angular distributions in transfer reactions, the orbital angular momentum l is revealed by the shape of the momentum distributions $P(\mathbf{k}_c)$. It is obvious, then, that the accuracy of the extracted spectroscopic factors, a measure of the occupancy of the single-particle orbitals in nuclei, and the conclusions that may follow from these spectroscopic factors about correlations inside nuclei depend in direct measure on the accuracy of the cross-section calculations. Similarly, the cross sections for one-proton-removal reactions $X \to Y + p$ are directly related to the nonresonant part of the astrophysical S factors for the inverse radiative proton capture $Y(p,\gamma)X$ (see, e.g., Refs. [4] and [6–9]). Again, the results and their reliability depend directly on the reliability and accuracy of the reaction calculations (as discussed in [10]).

The one-nucleon-removal cross section is calculated in most reaction models as an incoherent sum of the contributions of all core–single-particle configurations making the ground state of the fast-moving projectile

$$\sigma_{-1n} = \sum S(c; nlj)\sigma_{\rm sp}(nlj), \tag{1}$$

where $S(c; nlj)$ and $\sigma_{\rm sp}$ are the spectroscopic factors of each configuration and the single-particle-removal cross section, respectively [4]. A similar relation is valid for the momentum distributions. Systematic studies of projectiles and reactions allow the determination of the ordering, spacing, and occupancy of orbitals, essential in assessing how nuclei evolve in the presence of a large neutron or proton excess. Much work was done in this respect in the last decade in various laboratories. This information can be compared to many-body nuclear structure calculations, which are now able to reproduce the measured masses, charge radii, and low-lying excited states of a large number of nuclei. It was found that, e.g., for very exotic nuclei, the small additional stability that comes with the filling of a particular orbital can have profound effects upon their existence as bound systems, lifetime, and structure and can lead to the discovery of magic numbers that do not manifest along the valley of stability.

Extensions of the nucleon knockout formalism including the treatment of final-state interactions have been discussed

*mesutkarakoc@gmail.com

in Ref. [11], where it is shown that Coulomb final-state interactions are of relevance. In the meantime, the inclusion of higher-order effects [12,13] and a theory for two-nucleon knockout [14–16] have been developed. Knockout reactions represent a particular case for which higher projectile energies allow a simpler theoretical treatment of the reaction mechanism, owing to the simplicity of the reaction mechanism and the assumption of a single-step process.

A microscopic approach to direct reactions uses an effective nucleon-nucleon (NN) interaction (e.g., those in Ref. [17]) to start with. This interaction is often used to construct an optical potential with its imaginary part assumed to relate to the real part and its strength adjusted to reproduce experimental data. The real and imaginary parts of the potential can also be independent as in Refs. [6] and [7], where the procedure starts from an NN effective interaction with independent real and imaginary parts. For collisions at high energies ($E \gtrsim 100$), it is possible to show that, instead of NN interactions, one can use NN cross sections as the microscopic input [18]. In this case, an effective treatment of Pauli blocking of NN scattering is needed, as it manifests through medium modification of NN cross sections. It is well known that medium modification of the NN cross sections is necessary for an adequate numerical modeling of heavy-ion collision dynamics in central collisions. In these collisions, the ultimate purpose is to extract information about the nuclear equation of state by studying global collective variables describing the collision process. In direct reactions, such as one-nucleon removal reactions, medium effects of NN scattering are smaller because mostly low nuclear densities are probed. The first study of this effect in knockout reactions was carried out in Ref. [19]. Nonetheless, no comparison with experimental data was provided. In this work we explore further consequences of medium corrections and final-state interactions in knockout reactions. We study medium effects in the NN cross section in knockout reactions using the methods reported in Ref. [19], namely, with a geometrical treatment of Pauli blocking and with the Dirac-Brueckner theory in terms of baryon densities. We also explore the effect of final-state interaction, in particular, the effects of Coulomb distortion in the entrance and final reaction channels. This is of relevance as an increasing number of experiments use heavy targets with a large nuclear charge. We compare our results of knockout cross-section and momentum distribution calculations to a large number of published experimental data. The purpose is to improve the accuracy of the extracted spectroscopic factors that will lead to a better understanding of nuclear structure and to check and improve the reliability of the use of one-nucleon removal reactions as indirect methods in nuclear astrophysics.

II. MEDIUM AND DISTORTION EFFECTS

The geometrical treatment of Pauli corrections is performed using the isotropic NN scattering approximation because the numerical calculations can be largely simplified if we assume that the free NN cross section is isotropic. In this case, a formula which fits the numerical integration of the geometrical model reads [19]

$$\sigma_{\rm NN}(E,\rho_p,\rho_t)=\sigma_{\rm NN}^{\rm free}(E)\frac{1}{1+1.892\left(\frac{2\rho_<}{\rho_0}\right)\left(\frac{|\rho_p-\rho_t|}{\tilde\rho\rho_0}\right)^{2.75}}\times\begin{cases}1-\frac{37.02\tilde\rho^{2/3}}{E} & \text{if} \quad E>46.27\tilde\rho^{2/3},\\ \frac{E}{231.38\tilde\rho^{2/3}} & \text{if} \quad E\leqslant 46.27\tilde\rho^{2/3},\end{cases} \tag{2}$$

where E is the laboratory energy (in MeV), $\tilde\rho=(\rho_p+\rho_t)/\rho_0$, $\rho_<=\min(\rho_p,\rho_t)$, $\rho_{i=p,t}$ is the local density of nucleus i, and $\rho_0=0.17$ fm^{-3}. The parameters and models for the ρ_p and ρ_t densities which are used to describe the nuclei in this work are presented in Table I.

TABLE I. Ground-state densities from Refs. [26,27,29–31], where $r_{\rm ch}$ and r_m are the root mean square radii of the charge and nuclear matter densities, respectively.

Nucleus	Model	$\langle r_{\rm ch}^2\rangle^{1/2}$ (fm)	$\langle r_m^2\rangle^{1/2}$ (fm)	a (fm)	α (fm)
		Target			
^{9}Be	HO[a]	2.50(9)	2.367	1.77(6)	0.631
^{12}C	HO[b]	–	2.332	1.584	–
		Projectile-core			
^{10}Be	HO[a]	2.50(9)	2.372	1.77(6)	0.631
^{14}N	HO[a]	2.540(20)	2.410	1.729(6)	1.291
^{16}B	LDM[c]	–	–	–	–
^{22}Mg	HFB[d]	–	2.92	–	–
^{23}O	LDM[c]	–	–	–	–
^{32}Mg	HFB[d]	–	3.187	–	–

[a]Nuclear matter densities were obtained using the harmonic oscillator (HO) charge densities with parameters a and α from Ref. [26] and the method in Ref. [32].
[b]The HO nuclear matter density is from Ref. [27].
[c]LDM, liquid droplet model [28].
[d]HFB, Hartree-Fock-Bogoliubov. HFB calculations are from Refs. [29–31].

The Brueckner method goes beyond the simple geometrical treatment of Pauli blocking. Some of the Brueckner results that we used in this analysis have been reported in Refs. [20] and [21], where a simple parametrization is given. It reads (the misprinted factor 0.0256 in Ref. [21] has been corrected to 0.00256)

$$\sigma_{np}=[31.5+0.092|20.2-E^{0.53}|^{2.9}]\frac{1+0.0034E^{1.51}\rho^2}{1+21.55\rho^{1.34}},$$
$$\sigma_{pp}=[23.5+0.00256(18.2-E^{0.5})^{4.0}]\frac{1+0.1667E^{1.05}\rho^3}{1+9.704\rho^{1.2}}. \tag{3}$$

The limits of validity of this parametrization are clearly associated with the limits of validity of the Brueckner calculations, which are valid only below the pion-production threshold. A modification of this parametrization was introduced in Ref. [22] and consists in combining the free NN cross sections parametrized in Ref. [23] with the results of Brueckner theory reported in Refs. [20] and [21].

Current theoretical models for the calculation of momentum distributions and cross sections in high-energy nucleon-removal reactions follow a semiclassical probabilistic approach, described, e.g., in Refs. [24] and [25]. The method relies on the use of "survival amplitudes" (or S matrices) in the eikonal approximation,

$$S_i(b) = \exp[i\chi(b)] = \exp\left[-\frac{i}{\hbar v}\int_{-\infty}^{\infty} U_{i\mathrm{T}}(\mathbf{r})dz\right], \qquad (4)$$

where $r = \sqrt{b^2+z^2}$, and $U_{i\mathrm{T}}$ is the particle(i)-target(T) optical potential. In Ref. [18], a relation has been developed between the optical potential and the NN scattering amplitude. This relation is often referred to in the literature as the "t-$\rho\rho$ approximation." The t-$\rho\rho$ approximation is the basis of most calculations of elastic and inelastic scattering involving radioactive nuclei, as experimentally deduced optical potentials are not often available. In this approximation, the eikonal phase becomes

$$\chi(b) = \frac{1}{k_{\mathrm{NN}}}\int_0^{\infty} dq\, q\, \rho_p(q)\rho_t(q) f_{\mathrm{NN}}(q) J_0(qb), \qquad (5)$$

where $\rho_{p,t}(q)$ is the Fourier transform of the nuclear densities of the projectile and target, and $f_{\mathrm{NN}}(q)$ is the high-energy NN scattering amplitude at forward angles, which can be parametrized as

$$f_{\mathrm{NN}}(q) = \frac{k_{\mathrm{NN}}}{4\pi}\sigma_{\mathrm{NN}}(i+\alpha_{\mathrm{NN}})\exp(-\beta_{\mathrm{NN}}q^2). \qquad (6)$$

There are many ways of introducing final-state interactions in direct nuclear reactions, some of which are discussed in Refs. [11] and [33]. Besides Coulomb repulsion, included by modifying the straight-line trajectories accordingly, we have also modified the integral in Eq. (4) by using the optical potential including the Coulomb potential, which modifies the S matrices according to $S_i = S_i^N \cdot S_i^C$. The Coulomb phase in S_i^C is calculated by assuming a uniform charge distribution with radius R and is given by

$$\begin{aligned}\chi_C(b) = 2\eta\big\{&\Theta(b-R)\ln(kb) + \Theta(R-b)\\ &\times\big[\ln(kR) + \ln(1+\sqrt{1-b^2/R^2})\\ &-\sqrt{1-b^2/R^2} - \tfrac{1}{3}(1-b^2/R^2)^{3/2}\big]\big\}, \qquad (7)\end{aligned}$$

where Θ is the step function. The value R is chosen to be small enough so that the nuclear S matrices are basically 0 below $b = R$ because of the strong absorption at small impact parameters.

III. RESULTS AND DISCUSSION

In this section the results for momentum distributions and nucleon-removal cross sections are compared to several experimental data. The focus is the importance of medium corrections of NN cross sections and of Coulomb distortions. Both effects are expected to decrease as the bombarding energy increases. It is important to include such effects in order to minimize the uncertainty in the extraction of spectroscopic factors, especially at low bombarding energies. To substantiate this assertion, we analyze low-energy data on knockout reactions and compare them to high-energy data. In order to identify the separate contribution of these two factors, we do not vary the geometry of the nucleon binding potentials used to calculate the single-particle radial wave functions. This was identified in the literature as another major factor in the calculations leading to large variations in the extracted spectroscopic factors.

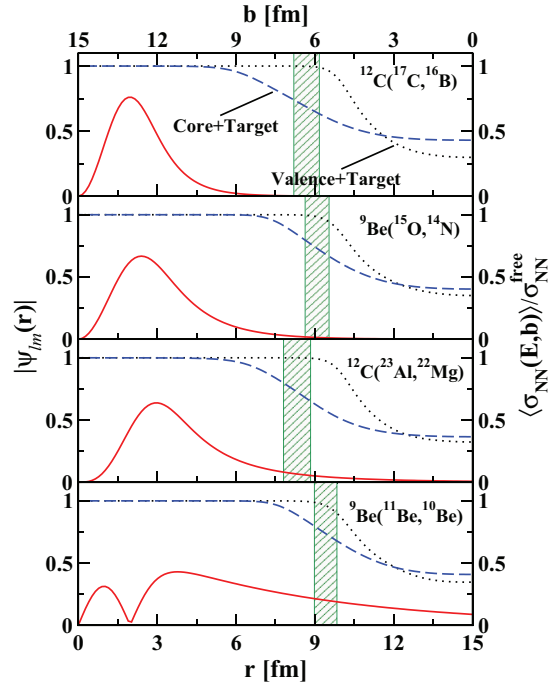

FIG. 1. (Color online) Top and right scale: Ratio between average in-medium and free nucleon-nucleon cross section as a function of the impact parameter. Dashed and dotted curves represent core-target and valence nucleon-target average nucleon-nucleon cross sections, respectively. Note that the target center of mass is located at the right of the top axis scale. Shaded areas represent the strong absorption radii where the knockout reactions most likely occur and $r_{\mathrm{sa}} = b_{\mathrm{sa}} = (1.1 \pm 0.1)(A_P^{1/3} + A_T^{1/3})$ fm. Bottom and left scale: Radial wave functions in arbitrary units (solid curves) for the valence nucleon-core system and for a few representative reactions considered in this work. We have taken only one configuration in cases of systems with multiple configurations.

The relevance of medium corrections is motivated by the effect summarized in Fig. 1. Cases shown in Fig. 1 are for ^{12}C(^{17}C,^{16}B) at 35 MeV/u, ^{9}Be(^{15}O,^{14}N) at 56 MeV/u, ^{12}C(^{23}Al,^{22}Mg) at 50 MeV/u, and ^{9}Be(^{11}Be,^{10}Be) at 60 MeV/u. Later we discuss more results for each system separately. Dashed and dotted curves show the ratio between the average in-medium and the free NN cross section as a function of the impact parameter (see top scale). We define the average NN cross section at the distance of closest approach between the projectile and the target using Eq. (2) and the definition

$$\langle\sigma_{\mathrm{NN}}(E,b)\rangle = \frac{\int d^3r_p\, \rho_p(\mathbf{r_p})\rho_t(\mathbf{r_p}+\mathbf{b})\,\sigma_{\mathrm{NN}}(E,\rho_p,\rho_t)}{\int d^3r \rho_p(\mathbf{r_p})\rho_t(\mathbf{r_p}+\mathbf{b})}, \qquad (8)$$

where **b** is the impact parameter vector, perpendicular to the beam axis.

In Fig. 1, dashed and dotted curves are for core-target and valence nucleon-target average NN cross sections, respectively. Note that the target center of mass is located at the right of the top axis scale. Also shown in the figure are the radial wave functions (solid curves) for the valence nucleon-core system and for a few representative reactions considered in this work. For simplicity, in Fig. 1 we have used only one of the main configurations for the projectile ground state (more detailed and complete calculations are reported later in this section). The binding energies "effectively" decrease from the top to the bottom panels. We say "effectively" because, although the binding energy of the valence proton in ^{23}Al is lower than for the valence neutron in ^{11}Be, the Coulomb barrier creates an effectively larger binding in ^{23}Al.

It is clearly noticeable in Fig. 1 that the wave functions of weakly bound systems extend far within the target where the NN cross sections are strongly modified by the medium. We must emphasize that the shaded areas in Fig. 1 are relevant to stress the importance of medium effects in the surface region, as the reaction is peripheral owing to strong absorption at $b < b_{sa}$. Momentum distributions and nucleon-removal cross sections in knockout reactions are thus expected to change appreciably with the inclusion of medium corrections of NN cross section. Such corrections are also expected to play a more significant role for loosely bound systems.

In the following, we discuss Coulomb corrections. Here we consider the simplest and most straightforward correction one can do, namely, the inclusion of a Coulomb phase, which accounts for the distortion of the elastic scattering of the core fragment. It has been usually taken for granted that longitudinal momentum distributions are little affected by elastic scattering of the core fragment, the reason being that the longitudinal forces acting on the core fragment reverse sign as the projectile passes by the target, leading to a reduced distortion effect [1]. Further, as shown in Ref. [11], the transverse momentum distributions are strongly affected by both nuclear and Coulomb elastic scattering. For heavier targets the distortions are predominantly caused by Coulomb repulsion [11]. It is noteworthy that the implications of the findings on Coulomb distortion effects presented in Ref. [11] have been neglected in the literature. In order to avoid dealing with the effects of the Coulomb scattering, experiments are usually performed with light targets, such as ^{9}Be, and at relatively high energies, $E \gtrsim 50$ MeV/nucleon. In this work we show that these arguments are not always valid and need to be studied with care.

As discussed in the previous section, in the presence of a Coulomb field the eikonal S matrices factorize as the product of the nuclear and the Coulomb contributions: $S(b) = S_n(b)S_C(b)$. Although this does not make any difference for the total stripping cross sections (see Eq. (20) in Ref. [19]), it has an impact on the diffraction dissociation cross section (through the second term of Eq. (21) in Ref. [19]). This means that not only the transverse, but also the longitudinal momentum distributions will be affected by the Coulomb field. This is shown in Fig. 2 for the longitudinal momentum distributions of several systems which we consider in detail later in this section.

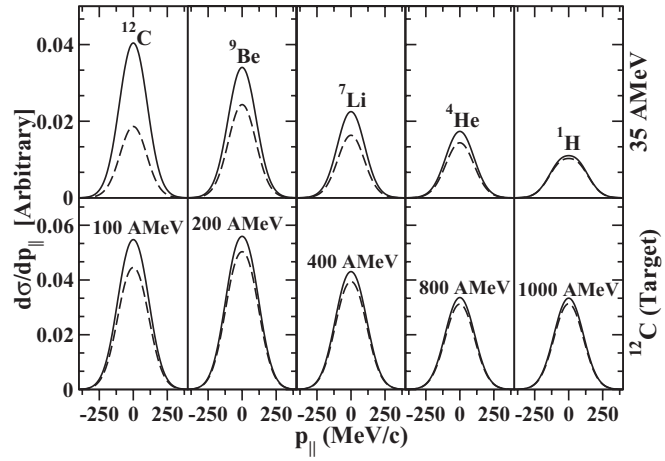

FIG. 2. Top: Display of Coulomb scattering effects in longitudinal momentum distributions for the reaction T(^{17}C,^{16}B)X at 35 MeV/u as a function of the target T. Solid (dashed) curves represent calculations with (without) Coulomb distortion. Bottom: Same as above, but for ^{12}C target and for different beam energies.

It is evident from the upper panels in Fig. 2 that longitudinal momentum distributions in knockout reactions T(^{17}C,^{16}B)X (and their total cross sections) are strongly influenced by the Coulomb field of the target T at bombarding energies of 35 MeV/nucleon. Solid (dashed) curves are calculations with (without) the inclusion of Coulomb scattering. It is also evident that, even for the case of light targets, such as ^{9}Be and ^{7}Li, the distributions change appreciably. The lower panels show calculations for the same reaction, but for ^{12}C targets and as a function of the bombarding energy. It is clear that distortions are important even for energies usually considered "safe," such as 100 MeV/nucleon.

We found that the effect of Coulomb scattering is relatively larger for systems of smaller sizes. This is illustrated in Fig. 3, where we present our calculations for the total

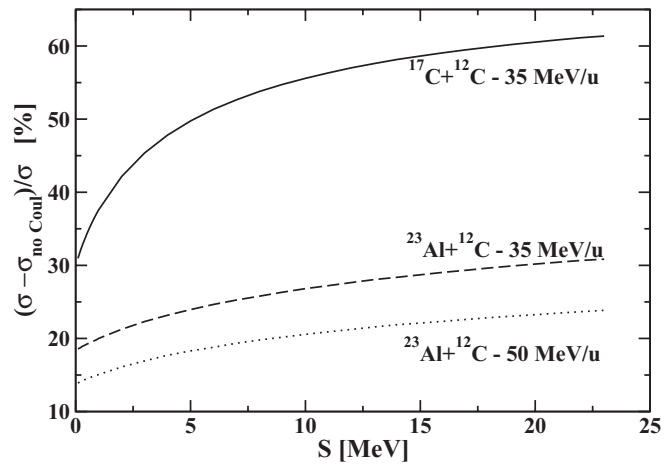

FIG. 3. Total nucleon removal cross sections for the reactions ^{12}C(^{17}C,^{16}B) (solid curve) and ^{12}C(^{23}Al,^{22}Mg) (dashed curve) at 35 MeV/u. We artificially vary the separation energy S of the proton in ^{17}C and in ^{23}Al. The dotted curve shows the calculation for ^{12}C(^{23}Al,^{22}Mg) at 50 MeV/u.

nucleon-removal cross sections for the reactions ^{12}C(^{17}C,^{16}B) (solid curve) and ^{12}C(^{23}Al,^{22}Mg) (dashed curve) at 35 MeV/u. We artificially vary the binding energy of the proton in ^{17}C and in ^{23}Al. As the separation energy increases, so does the percentage difference of the cross section, $(\sigma - \sigma_{\text{no Coul}})/\sigma$, where $\sigma_{\text{no Coul}}$ is a cross section without the Coulomb scattering phases. With increasing separation energy the relative valence nucleon-core distance decreases and the nucleon-removal cross section decreases, but the relative importance of the Coulomb scattering increases. For very low energies the effects of Coulomb dissociation (not considered here) should also become relevant and increase the magnitude of the cross sections. The relative importance of the Coulomb scattering for the removal cross sections decreases with the bombarding energy. This is shown in Fig. 3 with the calculation for ^{12}C(^{23}Al,^{22}Mg) at 50 MeV/u (dotted curve).

These preliminary discussions support our conclusion that both medium effects and Coulomb distortion play a relevant role in knockout reactions. Next we consider a series of published data for which neither medium nor Coulomb corrections were included. We thus quantify the changes in the extracted values of spectroscopic factors in case these effects are to be included in the experimental analysis.

A. ^{12}C(^{23}Al,^{22}Mg)X at 50 MeV/u

Recently, the ^{12}C(^{23}Al,^{22}Mg)X knockout reaction has been studied at 50 MeV/nucleon to investigate the ground-state properties of ^{23}Al [9]. It was shown that the ground-state structure of ^{23}Al is a configuration mixing of a d-orbital valence proton coupled to four core states of ^{22}Mg: 0^+_{gs}, 2^+_1, 4^+_1, and 4^+_2. The ground-state spin and parity of ^{23}Al as $J^\pi = 5/2^+$ have been confirmed. This experiment had the advantage that exclusive measurements were done and momentum distributions were determined for the four major configurations in the ground state of the projectile (^{23}Al).

In this work, we have analyzed the ^{12}C(^{23}Al,^{22}Mg)X system to check the relevance of Coulomb and medium effects. The $1d_{5/2}$ wave functions for the valence proton were generated in a spherical Woods-Saxon potential with the parameters listed in Table III.

In the optical limit of the Glauber theory and the t-$\rho\rho$ approximation (explained in detail in Refs. [17] and [18]), the eikonal phase is obtained from the input of the nuclear ground-state densities and the energy-dependent nucleon-nucleon cross sections. The ground-state density parameters and models used in this work are listed in Table I, and our results are presented in Fig. 4 and Table II.

To understand the effects of medium and Coulomb corrections, we have performed the calculations with different inputs. We show in Fig. 4 the calculations with both Coulomb and medium corrections (solid curve), calculations without any medium corrections (dashed lines), calculations that exclude Coulomb distortions but keep medium corrections (dashed-dotted curve), and calculations without either Coulomb or medium corrections (dotted curve).

The numerical results for the single-particle cross sections with different configurations are listed in Table II. For each of the four ^{22}Mg configurations—^{22}Mg - 0^+_{gs}, 2^+_1, 4^+_1, 4^+_2—the

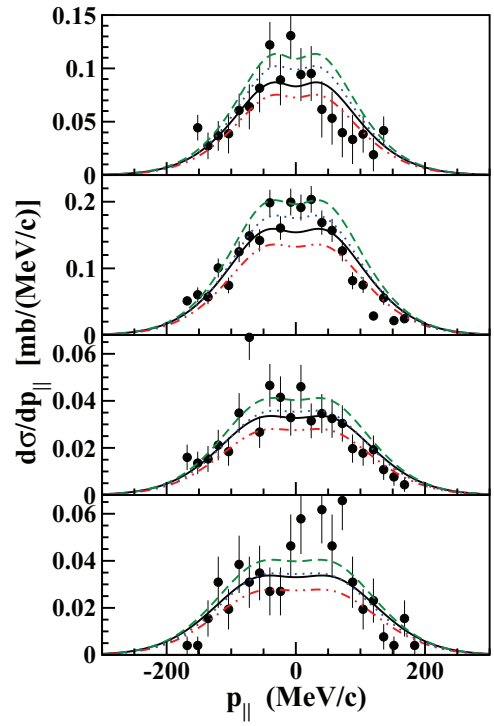

FIG. 4. (Color online) Comparison of experimental data in Ref. [9] and calculations for exclusive longitudinal momentum distributions in the knockout reaction ^{12}C(^{23}Al,^{22}Mg)X at 50 MeV/nucleon. The solid line includes both Coulomb and medium corrections. The dashed-curve includes no medium corrections. The dashed-dotted line includes calculations without Coulomb corrections. The dotted curve includes neither medium effects nor Coulomb corrections.

corresponding relative differences between full calculations and calculations without Coulomb corrections are found to be 15%, 17%, 19%, and 20%, respectively, whereas between full calculations and calculations without medium corrections the corresponding percentage differences are found to be 24%, 21%, 16%, and 13%, respectively.

B. ^{9}Be(^{15}O,^{14}N)X at 56 MeV/u

The one-proton-removal reaction from ^{15}O on a Be target has been measured at 56 MeV/nucleon and the total knockout cross section is reported as 80 ± 20 mb in Ref. [34]. The authors were able to explain the orbital occupancy of valence protons with a pure $1p_{1/2}$ single-particle state using a Glauber

TABLE II. Single-particle cross sections shown for each case separately.

Configuration	E_x	$\sigma_{sp}(nlj)$ (mb)			
	(keV)	Full	No medium correction	No Coulomb correction	Free
^{22}Mg$(0^+_{gs}) \otimes \pi_{1d_{5/2}}$	0	27.1	33.8	23.2	30.1
^{22}Mg$(2^+_1) \otimes \pi_{1d_{5/2}}$	1247	23.7	28.7	19.9	25.1
^{22}Mg$(4^+_1) \otimes \pi_{1d_{5/2}}$	3308	20.4	23.9	16.7	20.4
^{22}Mg$(4^+_2) \otimes \pi_{1d_{5/2}}$	5293	18.4	21.0	14.8	17.6

TABLE III. Bound-state potential parameters for the systems studied in the present work. r_0, r_{s0}, and r_c are the reduced radius of the bound-state potentials, where $r_i = R_i/A_p^{1/3}$ ($i = 0, s0, c$). S_{eff} is the effective separation energy: $S_{\text{eff}} = S_i + E_x^{\text{core}}$, where i = proton or neutron and E_x^{core} is the core excitation energy.

J_π	V_0 (MeV)	r_0 (fm)	a_0 (fm)	V_{s0} (MeV)	r_{s0} (fm)	a_{s0} (fm)	r_c (fm)	S_{eff} (MeV)
$\|^{10}\text{Be}(J^\pi)\otimes\nu 2s_{1/2}\rangle$								
$0^+_{(g.s)}$	61.13	1.21	0.52	–	–	–	1.21	0.504
$\|^{14}\text{N}(J^\pi)\otimes\pi nlj\rangle$								
$1^+_{(g.s)}(1p1/2)$	48.36	1.19	0.60	–	–	–	1.19	7.297
$1^+_{(g.s)}(1p3/2)$	48.36	1.19	0.60	–	–	–	1.19	7.297
$\|^{16}\text{B}(J^\pi)\otimes\pi 1p_{3/2}\rangle$								
$0^+_{(g.s)}$	79.46	1.09	0.50	35.0	1.09	0.50	1.09	23.330
3^-_1	80.35	1.09	0.50	35.0	1.09	0.50	1.09	23.979
2^-_1	80.75	1.09	0.50	35.0	1.09	0.50	1.09	24.273
2^-_2	81.85	1.09	0.50	35.0	1.09	0.50	1.09	25.078
1^-_1	82.17	1.09	0.50	35.0	1.09	0.50	1.09	25.318
3^-_2	79.93	1.09	0.50	25.0	1.09	0.50	1.09	26.066
$\|^{22}\text{Mg}(J^\pi)\otimes\pi 1d_{5/2}\rangle$								
$0^+_{(g.s)}$	54.60	1.18	0.60	5.0	1.18	0.60	1.18	0.141
2^+	56.96	1.18	0.60	5.0	1.18	0.60	1.18	1.388
4^+_1	60.67	1.18	0.60	5.0	1.18	0.60	1.18	3.449
4^+_2	64.07	1.18	0.60	5.0	1.18	0.60	1.18	5.434
$\|^{23}\text{O}(J^\pi)\otimes\nu 2s_{1/2}\rangle$								
$1/2^+_{(g.s)}$	42.40	1.27	0.70	–	–	–	1.27	3.610
$\|^{32}\text{Mg}(J^\pi)\otimes\nu nlj\rangle$								
$0^+_{(g.s)}(1d_{3/2})$	–	–	–	–	–	–	–	2.21
$3^-(2p_{3/2})$	79.92	1.04	0.70	10.0	1.03	0.70	1.04	5.07
$3^-(1f_{7/2})$	86.63	1.04	0.70	10.0	1.03	0.70	1.04	5.07
$2^+_2(2s_{1/2})$	51.55	1.04	0.70	10.0	1.03	0.70	1.04	5.22

reaction model. Their calculations imply that the $1p_{3/2}$ state could also have a small contribution because the calculations with only the $1p_{1/2}$ state yield a narrower momentum distribution than observed in the experiment. The physical implication of this is a possible knockout from more deeply bound protons in the $1p_{3/2}$ state. The contributions from each of the p states yield spectroscopic factors of 1.27(9) and 0.100(75) for the $1p_{1/2}$ and the $1p_{3/2}$ orbitals, respectively (Ref. [34] and references therein).

We have followed the interpretation of Ref. [34] and calculated the one-proton-removal cross sections for the same reaction with the same orbital occupancy assumption. The parameters are listed in Tables I and III. Our calculations with both Coulomb and medium corrections, upon slightly changing the spectroscopic factors to 1.42 and 0.13, are in agreement with the results in Ref. [34]. The calculated one-proton-removal cross sections are 78.79, 75.20, 93.98, and 90.74 mb with both Coulomb and medium corrections, no Coulomb corrections, no medium corrections, and neither medium effects nor Coulomb corrections, respectively. The difference between full calculations, including medium and Coulomb scattering effects, and calculations without Coulomb corrections is of the order of 5%, and that between full calculations and calculations without medium effects is nearly 19%. This is remarkable even though it again fits within the error of the total knockout cross-section experimental data. We thus conclude that, for this case, medium effects and Coulomb distortion do not have a sizable impact on the extraction of spectroscopic factors. However, one can easily see from Fig. 5 that the data show an asymmetry which can

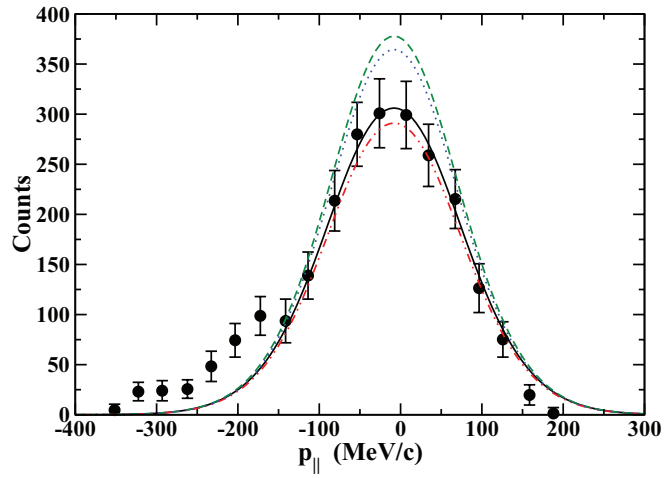

FIG. 5. (Color online) Longitudinal momentum distributions for the ^{9}Be(^{15}O,^{14}N)X reaction at 56 MeV/u. Solid lines represent calculations that include both Coulomb and medium corrections. Dashed lines stem from calculations that do not include medium corrections. Calculations denoted by dashed-dotted curves are performed without Coulomb corrections. The dotted curve does not include medium effects or Coulomb corrections. Data are taken from Ref. [34].

only be explained with the inclusion of higher-order effects in the reaction mechanism. Distortions will be manifest owing to continuum-continuum coupling of states involving the interaction of core with the valence proton. These mechanisms are not considered in the present work.

C. ^{12}C(^{17}C,^{16}B)X at 35 MeV/u

1. Transverse momentum distributions

The one-proton-removal reaction from ^{17}C, with a separation energy of 23 MeV, has been measured in the reaction ^{12}C(^{17}C,^{16}B)X at 35 MeV/nucleon with the goal of understanding the low-lying structure of the unbound ^{16}B nucleus. Using this reaction, Ref. [35] studied the unbound $^{15}\mathrm{B}+n$ system with the assumption of a d-wave neutron decay. Our interest is to compute the transverse momentum distribution of the ^{16}B fragment following the same assumptions as in Ref. [35] in order to study the consequences of medium and Coulomb corrections. The configuration of the proton removed from ^{17}C is assumed to be

$$\begin{aligned}|^{17}\mathrm{C}\rangle = {} & \alpha_1|^{16}\mathrm{B}(0^-)\otimes\pi 1p_{3/2}\rangle \\ & +\alpha_2|^{16}\mathrm{B}(3_1^-)\otimes\pi 1p_{3/2}\rangle+\alpha_3|^{16}\mathrm{B}(2_1^-)\otimes\pi 1p_{3/2}\rangle \\ & +\alpha_4|^{16}\mathrm{B}(2_2^-)\otimes\pi 1p_{3/2}\rangle+\alpha_5|^{16}\mathrm{B}(1_1^-)\otimes\pi 1p_{3/2}\rangle \\ & +\alpha_6|^{16}\mathrm{B}(3_2^-)\otimes\pi 1p_{3/2}\rangle, \end{aligned} \quad (9)$$

where α_i is the spectroscopic amplitude for a core–single-particle configuration $i=(c\otimes nlj)$.

Using spectroscopic factors obtained by means of a shell-model calculation with the WBP interaction [36], Ref. [35] obtained a good agreement between data and calculated transverse momentum distributions. But the measured total cross section is 6.5(1.5) mb, versus the theoretical result of 24.7 mb. The explanation for this large difference is proposed in Ref. [37] as a reduction of the spectroscopic factor by 70% for strongly bound nucleon systems. After this spectroscopic reduction is accounted for, the theoretical estimates for the cross section becomes 7.5 mb, in reasonable accordance with the data.

In the present work, we do not elaborate on the assumption introduced in Ref. [35], and we use the same configuration and spectroscopic factors as in [35]. The proton binding potential parameters listed in Table III are adjusted to obtain the effective separation energies. The ground-state densities are also listed in Table I. Here, as shown in Fig. 6, we find that medium corrections change the total knockout cross sections by 5%, but the Coulomb corrections have a very large effect, which is almost 60% between calculations with Coulomb and those without Coulomb distortion. The reason for this difference is that the Coulomb distortion and repulsion effectively increase the collision distance with the small impact parameters needed to remove a strongly bound nucleon. This was not observed in the previous case [^{9}Be(^{15}O,^{14}N)X at 56 MeV/u] because of the small nuclear binding in that case. We have also observed that this effect sharply reduces the calculated cross sections and the removal is more effective as the bombarding energy decreases.

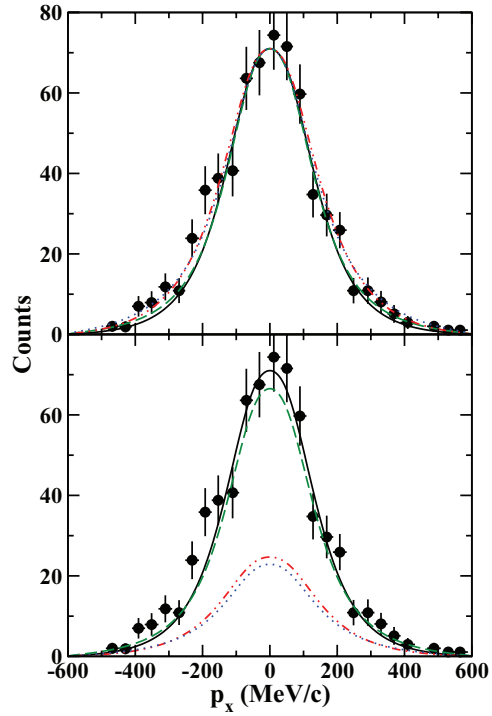

FIG. 6. (Color online) Transverse momentum distributions for the ^{12}C(^{17}C,^{16}B)X system at 35 MeV/u. Solid lines represent calculations including both Coulomb and medium corrections. Dashed lines stem from calculations that do not include medium corrections. Calculations represented by dashed-dotted curves are performed without Coulomb corrections. The dotted curve does not include medium effects or Coulomb corrections. Data are taken from Ref. [35]. Top: One can see that, when properly scaled, all four curves from the calculations reproduce the shape of the momentum distributions. Bottom: Relative differences of our results are illustrated when the full calculation (solid line) is scaled to the data.

2. Longitudinal momentum distributions

We have made a more systematic analysis to understand the reason for the effect discussed in the previous subsection. We have observed that the strong dependence on Coulomb distortions is also present in longitudinal momentum distributions. It has long been thought that longitudinal momentum distributions are free from uncertainties related to the knowledge of the optical nucleus-nucleus potentials compared to the transverse distributions. This was first shown in Ref. [1]. Here we report calculations for the same $|^{16}\mathrm{B}(0^-)\otimes\pi 1p_{3/2}\rangle$ configuration, with the same parameters and ground-state densities, as discussed in the previous subsection. We find that although the Coulomb distortions create a similar effect for this particular knockout reaction on both transverse and longitudinal momentum distributions, as shown in Fig. 2, the effect on transverse momentum distributions is bigger than the corresponding one for longitudinal momentum distributions, by about 5%. This is expected on physics grounds. Nonetheless, such a large effect on longitudinal momentum distributions was not initially anticipated. By comparison with other cases, we found that this large effect is caused by the low bombarding energy in this particular reaction combined with

the large binding energy of the projectile. This interpretation is also validated by inspection of Figs. 2 and 3.

The source of this difference stems from the diffraction dissociation contribution to the cross sections. To substantiate our claim, we have looked at the details of the knockout cross section, which has two parts for the production of a given final state of the residue. The most important of the two, commonly referred to as stripping or inelastic breakup, represents all events in which the removed nucleon reacts with and excites the target from its ground state. The second component, called diffractive or elastic breakup [38], represents the dissociation of the nucleon from the residue through their two-body interactions with the target, each being elastically scattered. We note that the total stripping cross section is given by [11]

$$\sigma_{\rm str} = S(c;nlj)\frac{2\pi}{2l+1}\sum_m \int_0^\infty db_n\, b_n\, [1-|S_n(b_n)|^2] \times \int d^3r\, |S_c(b_c)|^2 |\psi_{lm}(\mathbf{r})|^2, \quad (10)$$

whereas the integrated diffraction dissociation cross section is given by [33]

$$\sigma_{\rm dif} = S(c;nlj)\frac{2\pi}{2l+1}\sum_m \int_0^\infty db_n\, b_n \times \left\{ \int d^3r |S_n(b_n)S_c(b_c)\psi_{lm}(\mathbf{r})|^2 - \sum_{m'} \left| \int d^3r \psi_{lm'}(\mathbf{r}) S_c(b_c) S_n(b_n) \psi_{lm}(\mathbf{r}) \right|^2 \right\}. \quad (11)$$

One can see from these expressions that the stripping cross sections are not affected by the Coulomb distortions because this distortion is manifest through a real phase in the eikonal S matrices calculated in the Glauber approximation. The magnitude of the cross sections is therefore not changed, as the square of the S matrices entering Eq. (10) is only changed by the imaginary part of the potential entering Eq. (4). On the other hand, the second term of the diffraction dissociation cross sections in Eq. (11) is appreciably modified by the Coulomb phase factor. As shown in Fig. 2, the effect gets smaller with decreasing target atomic number, because the Coulomb phase increases, or when the beam energy increases, because then the Coulomb recoil becomes irrelevant.

D. ^{9}Be(^{11}Be,^{10}Be)X at 60 MeV/u

In order to further understand the dependence of the Coulomb distortion on nuclear binding, we consider the reaction ^{9}Be(^{11}Be,^{10}Be)X at 60 MeV/u, which can be modeled by a core-plus-valence system with the assumption $^{10}\mathrm{Be}_{\rm gs}(0^+) + \mathrm{n}$ in the $2s_{1/2}$ orbital for the ground state of $^{11}\mathrm{Be}_{\rm gs}(1/2^+)$ ($S_n = 0.504$ MeV). Here we use the same Woods-Saxon potential parameters for the bound state as published in Ref. [25]: ($R_0 = 2.70$ fm, $a_0 = 0.52$ fm). In Fig. 7 and Table IV we present our results for the neutron-removal longitudinal momentum distribution of 60 MeV/nucleon ^{11}Be projectiles incident on ^{9}Be targets.

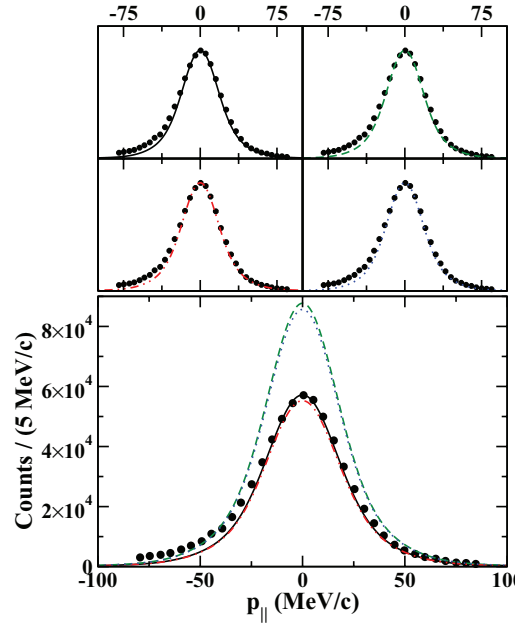

FIG. 7. (Color online) Longitudinal momentum distributions of the reaction ^{9}Be(^{11}Be,^{10}Be) at 60 MeV/nucleon. Solid lines represent calculations that include both Coulomb and medium corrections. Dashed lines stem from calculations that do not include medium corrections. Calculations denoted by dashed-dotted curves are performed without Coulomb corrections. The dotted curve does not include medium effects or Coulomb corrections. Data are taken from Ref. [39]. Top: One can see that, when properly scaled, all four curves from the calculations reproduce the shape of the momentum distributions. Bottom: Relative differences of our results are illustrated when the full calculation (solid line) is scaled to the data.

It is evident from Fig. 1 that ^{17}C has the smallest "effective" size and that ^{11}Be has the biggest size among the low-energy systems in this study. The nuclear size is important for low-energy cases because diffraction dissociation becomes dominant when the nuclear size is smaller, but stripping dissociation becomes dominant when the nuclear size is bigger. The reason for this is that a large projectile feels the nuclear interaction already at large impact parameters. A small projectile can come closer to the target where the Coulomb interaction is larger. The evidence of this is presented in Table IV. It is thus clear why medium and Coulomb corrections are more important in the ^{9}Be(^{11}Be,^{10}Be) and the ^{12}C(^{17}C,^{16}B) cases, respectively.

E. ^{12}C(^{24}O,^{23}O)X at 920 MeV/u

The momentum distribution of the one-neutron removal residues from the ^{12}C(^{24}O,^{23}O)X reaction was measured for the first time at 920 MeV/nucleon and reported in Ref. [40]. The data can be explained by the spectroscopic factor $S = 1.74(19)$ of an almost-pure $2s_{1/2}$ single-particle state for the valence neutron. This work, together with recent theoretical calculations, suggests that ^{24}O is a newly discovered doubly magic nucleus. The one-neutron-removal cross section was found to be 63(7) mb. Calculations in Ref. [40] were based

TABLE IV. Cross sections (in mb) calculated for the systems ^{12}C(^{17}C,^{16}B) at 35 MeV/nucleon and ^{9}Be(^{11}Be,^{10}Be) at 60 MeV/nucleon.

$\sigma_{-1n} = \sigma_{\rm dif} + \sigma_{\rm str}$	^{12}C(^{17}C,^{16}B)			^{9}Be(^{11}Be,^{10}Be)		
	Full	No Coulomb correction	No medium correction	Full	No Coulomb correction	No medium correction
Strip.	7.10	7.10	5.09	126.5	126.5	169.7
Diff.	18.63	2.42	19.39	52.8	46.7	104.8
Total	25.74	9.52	24.48	179.3	173.2	274.5

on a few-body Glauber formalism [41] for two configurations: (a) $^{23}O_{gs}(1/2^+)$ + n in the $2s_{1/2}$ orbital and (b) $^{23}O_{gs}(5/2^+)$ + n in the $1d_{5/2}$ orbital. The wave functions for the configurations are obtained with a Woods-Saxon potential by adjusting the depth of the potential to reproduce the one-neutron separation energy $S_n = 3.61(27)$ MeV [29]. Using a pure $2s_{1/2}$ configuration with $S = 1$ leads to a cross section of 34 mb. The calculation is in agreement with the data when it is multiplied by $S = 1.74(19)$. This large spectroscopic factor indicates that the single-particle strength of the valence neutron is strongly weighted in the $2s_{1/2}$ state.

In the present work we have reproduced the data of Ref. [40] also by assuming a $2s_{1/2}$ orbital only. The potential parameters for the bound-state wave function are given in Table III and the ground-state density for the $^{23}O_{gs}$ core is obtained using liquid droplet model densities [42], as indicated in Table I. To understand the differences between medium effect models, four different calculations including Coulomb corrections have been made for this system. The calculated one-neutron-removal cross sections are 58.58, 54.08, 78.74, and 53.25 mb using free [19], Pauli-corrected [Eq. (2)], Brueckner [Eq. (3)], and phenomenological parameterizations [22] of the NN cross sections, respectively. Except for the result obtained with the Brueckner theory, they are all in agreement with the previous work and with the data. The relative difference between the results obtained using Brueckner corrections and with free NN cross sections is about 34%. However, we do not consider a real discrepancy, as the Brueckner parametrizations have been extrapolated well beyond their validity. Brueckner calculations are limited by the pion-production threshold and should only be valid for projectile energies below 300 MeV/nucleon.

Thus we verify that the experimental data for the reaction ^{12}C(^{24}O,^{23}O)X at 920 MeV/u is well reproduced with the use of free NN cross sections (Fig. 8). The changes introduced by Pauli blocking with the geometric model are small, and the phenomenological account of medium effects at this high energy also basically agree with the results using free cross sections.

F. ^{12}C(^{33}Mg,^{32}Mg)X at 898 MeV/u

The ground-state structure of ^{33}Mg, a nucleus belonging to the $N = 20$ island of inversion, has been studied in Ref. [43] by means of nucleon-removal reactions on a carbon target at 898 MeV/nucleon. The longitudinal momentum distribution of the ^{32}Mg core was measured and the one-neutron-removal cross section was found to be 74(4) mb. Most of the contribution to the ground-state structure of ^{33}Mg was shown to arise from the $2p_{3/2}$ orbital.

The longitudinal momentum distribution obtained in Ref. [43] cannot be reproduced with a pure single-particle state (Fig. 9). Why a configuration mixing of different single-particle states is needed has been discussed in detail in Ref. [43]. Two different configuration mixings for the ground state of ^{33}Mg were assumed. The first one is

$$\begin{aligned}|^{33}\mathrm{Mg}_{gs}(3/2^-)\rangle &= \alpha_1|^{32}\mathrm{Mg}(2_1^+)\otimes\nu 2p_{3/2}\rangle + \alpha_2|^{32}\mathrm{Mg}(1^-)\otimes\nu 2s_{1/2}\rangle \\ &+ \alpha_3|^{32}\mathrm{Mg}(2_1^+)\otimes\nu 1f_{7/2}\rangle + \alpha_4|^{32}\mathrm{Mg}(1^-)\otimes\nu 1d_{3/2}\rangle \\ &+ \alpha_5|^{32}\mathrm{Mg}(\mathrm{gs})\otimes\nu 2\mathrm{p}_{3/2}\rangle, \end{aligned} \quad (12)$$

and the second is

$$\begin{aligned}|^{33}\mathrm{Mg}_{gs}(3/2^+)\rangle &= \alpha_1|^{32}\mathrm{Mg}(3^+)\otimes\nu 2p_{3/2}\rangle + \alpha_2|^{32}\mathrm{Mg}(2_2^+)\otimes\nu 2s_{1/2}\rangle \\ &+ \alpha_3|^{32}\mathrm{Mg}(3^+)\otimes\nu 1f_{7/2}\rangle + \alpha_4|^{32}\mathrm{Mg}(\mathrm{gs})\otimes\nu 1\mathrm{d}_{3/2}\rangle, \end{aligned} \quad (13)$$

where α_i are the spectroscopic amplitudes for each single-particle orbital. The values of the corresponding spectroscopic factor S_i were found by χ^2 minimization and their values for the second configuration are $S_1 = 2.2^{+0.2}_{-0.5}$, $S_2 = 0.1^{+0.0}_{-0.1}$, $S_3 = 1.1^{+0.1}_{-0.5}$, and $S_4 = 0.0^{+0.5}_{-0.0}$ [43].

In our calculations we have chosen the second configuration set used in Ref. [43], Eq. (13), since the ^{33}Mg ground

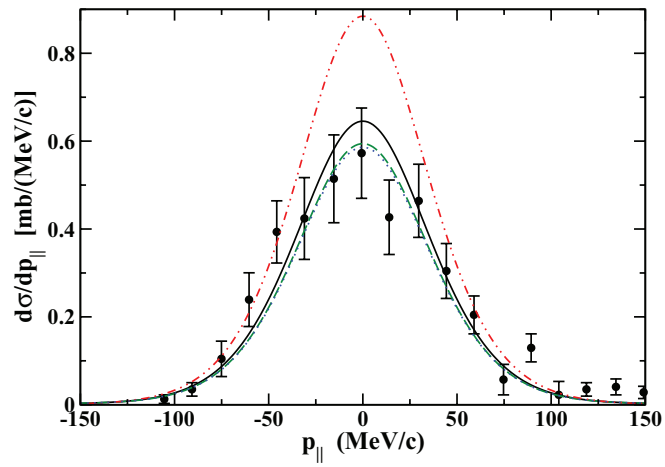

FIG. 8. (Color online) Longitudinal momentum distributions for the ^{12}C(^{24}O,^{23}O)X reaction at 920 MeV/nucleon. Curves were calculated with the free NN cross sections (solid), a geometrical account of Pauli blocking (dashed), a phenomenological fit from Ref. [22] (dotted), and a correction from Brueckner theory (dashed-dotted). Data are taken from Ref. [40].

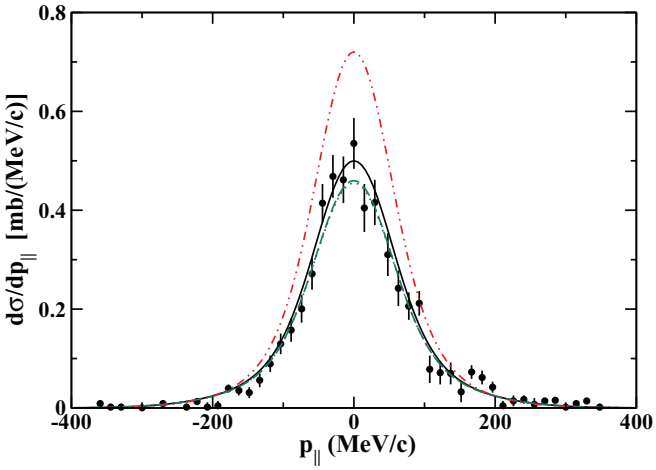

FIG. 9. (Color online) Inclusive longitudinal momentum distributions for the ^{12}C(^{33}Mg,^{32}Mg)X system at 898 MeV/nucleon. Data are taken from Kanungo *et al.* [43]. Curves were calculated with the free NN cross sections (solid), a geometrical account of Pauli blocking (dashed), a phenomenological fit from Ref. [22] (dotted), and a correction from Brueckner theory (dashed-dotted).

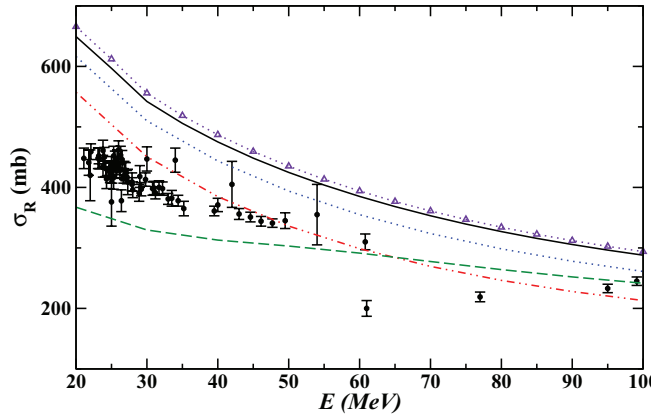

FIG. 10. (Color online) Total reaction cross section of p+^{12}C taken from Ref. [44]. Curves were calculated with the free NN cross sections from Ref. [45] (solid), a geometrical account of Pauli blocking (dashed), a phenomenological fit from Ref. [22] (dotted), and a correction from Brueckner theory (dashed-dotted). The triangle-dotted curve is calculated with the same free NN cross sections from Ref. [45] but with another HFB calculation [46] for the ^{12}C ground-state density.

state is usually accepted to be $J^\pi = 3/2^+$. We apply the same procedure as described before to obtain bound-state wave functions and eikonal phases. The parameters for the bound-state potentials and ground-state densities are listed in Tables III and I, respectively. We have used nearly the same spectroscopic factors within the error bar range of Ref. [43] to make a consistent comparison of the medium effects. Our results yield a small but relevant variation of the one-neutron removal cross sections using the free, Pauli-corrected, and phenomenological NN cross sections, namely, 83.70, 77.90, and 77.63 mb, respectively. As observed in the case of the ^{12}C(^{24}O,^{23}O)X at 920 MeV/u, the use of Brueckner-corrected NN cross sections yields 112.92 mb, about 35% relative to the calculations using the free NN cross sections (Fig. 9). For the same reason as for the previously considered reaction, this discrepancy is meaningless, as one extrapolates the Brueckner results beyond their regime of validity.

Both reactions considered above are very illustrative, as they show a great consistency between the calculations performed by different authors, with somewhat different methods. They also show the expected relevance of medium corrections for intermediate- and low-energy collisions.

G. Relevance of medium effects

As mentioned above, medium effects have been routinely neglected in the experimental analysis of knockout reactions. But their relevance has been known for a long time in the analysis of elastic and inelastic scattering, as well as of total reaction cross sections [17,18]. The effects are larger at lower bombarding energies, where Pauli blocking strongly reduces the NN cross sections in the medium. A systematic study of these effects has been presented in Ref. [18].

To corroborate these statements, in Fig. 10 we show the data on the p+^{12}C reaction cross sections taken from the Ref. [44] in the energy region of our interest, 20–100 MeV/nucleon. The cross sections were calculated from the relation

$$\sigma_R = 2\pi \int db\, b[1 - |S(b)|^2], \tag{14}$$

where $S(b)$ has been calculated using Eqs. (4)–(6) and the carbon matter density from a Hartree-Fock-Bogoliubov (HFB) calculation [46]. Several distinct calculations are shown. The solid curve uses Eq. (5) with the free NN cross sections and the carbon matter density from an HFB calculation [47], whereas the triangle-dotted curve (the triangles are not data but are used for better visibility) uses a different HFB density [46], consistent with the calculations presented in Ref. [7]. As expected, the agreement between the two calculations is very good.

The other curves in Fig. 10 show the same calculation procedure, but including medium corrections for the NN cross section. The results are evidently very different from the previous ones. The dotted, dashed-dotted, and dashed curves use phenomenological, Brueckner, and Pauli geometrical recipes, respectively, for medium effects on the cross sections. Based on the large error bars and spread of the experimental data, it is hard to judge which model adopted for medium corrections yields the best agreement with the data. It is clear that the inclusion of medium effects changes the results to yield a closer reproduction of the data.

These findings are in agreement with our present understanding of medium modifications of the reaction cross sections and of several other reaction channels involving heavy-ion scattering at intermediate energies (∼50 MeV/nucleon).

IV. CONCLUSIONS

Often neglected effects, such as medium modifications of NN cross sections and Coulomb distortion, modify appreciably the nucleon knockout cross sections. As we have shown, these effects do not lead to an appreciable modification of

the shapes of momentum distributions. This is explained by the fact that the momentum distributions are largely the Fourier transforms of the contributing parts of the single-particle wave functions, overwhelmingly their asymptotic regions, which are the Whittaker functions for protons or the Hankel functions for neutrons, sensitive only to the orbital momentum and the nucleon binding energies. We have shown these features explicitly by comparing our results with a large number of available experimental data. As expected on physics grounds, these corrections are larger for experiments at lower energies, around 50 MeV/nucleon, and for heavy targets.

As more experiments make use of heavier targets, it is worthwhile to illustrate the relevance of Coulomb corrections. Medium effects in knockout reactions have also been frequently ignored in the past. We show that they also have to be included in order to obtain a better accuracy of the extracted spectroscopic factors. Although these conclusions might not come as a big surprise, they have not been properly included in many previous experimental analyses.

ACKNOWLEDGMENTS

This work was partially supported by US Department of Energy Grant Nos. DE-SC004972, DE-FG02-08ER41533, and DE-FG02-10ER41706 and by the Research Corporation. M. Karakoç was also partially supported by TUBITAK Grant No. 109T373.

[1] C. A. Bertulani and K. W. McVoy, Phys. Rev. C **46**, 2638 (1992).
[2] P. G. Hansen, Nature **334**, 194 (1998).
[3] J. A. Tostevin, J. Phys. G **25**, 735 (1999).
[4] P. G. Hansen and J. A. Tostevin, Annu. Rev. Nucl. Part. Sci. **53**, 219 (2003).
[5] A. Gade, P. Adrich, D. Bazin, M. D. Bowen, B. A. Brown, C. M. Campbell, J. M. Cook, T. Glasmacher, P. G. Hansen, K. Hosier, S. McDaniel, D. McGlinchery, A. Obertelli, K. Siwek, L. A. Riley, J. A. Tostevin, and D. Weisshaar, Phys. Rev. C **77**, 044306 (2008).
[6] L. Trache, F. Carstoiu, C. A. Gagliardi, and R. E. Tribble, Phys. Rev. Lett. **87**, 271102 (2001).
[7] L. Trache, F. Carstoiu, A. M. Mukhamedzhanov, and R. E. Tribble, Phys. Rev. C **66**, 035801 (2002).
[8] P. Navratil, C. A. Bertulani, and E. Caurier, Phys. Rev. C **73**, 065801 (2006).
[9] A. Banu *et al.*, Phys. Rev. C **84**, 015803 (2011).
[10] L. Trache, F. Carstoiu, C. A. Gagliardi, and R. E. Tribble, Phys. Rev. C **69**, 032802(R) (2004).
[11] C. A. Bertulani and P. G. Hansen, Phys. Rev. C **70**, 034609 (2004).
[12] B. Abu-Ibrahim and Y. Suzuki, Phys. Rev. C **61**, 051601(R) (2000).
[13] B. Abu-Ibrahim, Y. Ogawa, Y. Suzuki, and I. Tanihata, Comp. Phys. Comm. **151**, 369 (2003).
[14] J. A. Tostevin and B. A. Brown, Phys. Rev. C **74**, 064604 (2006).
[15] E. C. Simpson, J. A. Tostevin, D. Bazin, B. A. Brown, and A. Gade, Phys. Rev. Lett. **102**, 132502 (2009).
[16] E. C. Simpson, J. A. Tostevin, D. Bazin, and A. Gade, Phys. Rev. C **79**, 064621 (2009).
[17] L. Ray, Phys. Rev. C **20**, 1857 (1979).
[18] M. S. Hussein, R. A. Rego, and C. A. Bertulani, Phys. Rep. **201**, 279 (1991).
[19] C. A. Bertulani and C. De Conti, Phys. Rev. C **81**, 064603 (2010).
[20] G. Q. Li and R. Machleidt, Phys. Rev. C **48**, 1702 (1993).
[21] G. Q. Li and R. Machleidt, Phys. Rev. C **49**, 566 (1994).
[22] X. Cai, J. Feng, Jun, W. Shen, Y. Ma, J. Wang, and W. Ye, Phys. Rev. C **58**, 572 (1998).
[23] S. K. Charagi and S. K. Gupta, Phys. Rev. C **41**, 1610 (1990).
[24] M. S. Hussein and K. W. McVoy, Nucl. Phys. A **445**, 124 (1985).
[25] K. Hencken, G. Bertsch, and H. Esbensen, Phys. Rev. C **54**, 3043 (1996).
[26] H. De Vries, C. W. de Jager, and C. De Vries, At. Data Nucl. Data Tables **36**, 495 (1987).
[27] D. T. Khoa, Phys. Rev. C **63**, 034007 (2001).
[28] W. D. Myers, Nucl. Phys. A **145**, 387 (1970).
[29] G. Audi, A. H. Wapstra, and C. Thibault, Nucl. Phys. A **729**, 337 (2003).
[30] S. Goriely, M. Samyn, and J. M. Pearson, Phys. Rev. C **75**, 064312 (2007).
[31] I. Angeli, At. Data Nucl. Data Tables **87**, 185 (2004).
[32] G. R. Satchler and W. G. Love, Phys. Rep. **55**, 183 (1979).
[33] C. A. Bertulani and A. Gade, Comp. Phys. Comm. **175**, 372 (2006).
[34] H. Jeppesen *et al.*, Nucl. Phys. A **739**, 57 (2004).
[35] J.-L. Lecouey *et al.*, Phys. Lett. B **672**, 6 (2009).
[36] E. K. Warburton and B. A. Brown, Phys. Rev. C **46**, 923 (1992).
[37] A. Gade *et al.*, Phys. Rev. Lett. **93**, 042501 (2004).
[38] C. A. Bertulani and G. Baur, Nucl. Phys. A **480**, 615 (1988).
[39] T. Aumann *et al.*, Phys. Rev. Lett. **84**, 35 (2000).
[40] R. Kanungo *et al.*, Phys. Rev. Lett. **102**, 152501 (2009).
[41] Y. Ogawa, Y. Suzuki, and K. Yabana, Nucl. Phys. A **571**, 784 (1994).
[42] W. D. Myers and W. J. Swiatecki, Ann. Phys. **55**, 395 (1969); **84**, 186 (1974).
[43] R. Kanungo *et al.*, Phys. Lett. B **685**, 253 (2010).
[44] R. F. Carlson, At. Data Nucl. Data Tables **63**, 93 (1996).
[45] S. John, L. W. Townsend, J. W. Wilson, and R. K. Tripathi, Phys. Rev. C **48**, 766 (1993).
[46] M. Beiner and R. J. Lombard, Ann. Phys. (NY) **86**, 262 (1974); F. Carstoiu and R. J. Lombard, *ibid.* **217**, 279 (1992).
[47] http://www.nscl.msu.edu/∼brown/resources/resources.html